International Journal of Dairy Technology

SDT Society of Dairy Technology

Check for updates

doi: 10.1111/1471-0307.70086

RESEARCH ARTICLE

Defining the role of the locking point in spray drying by using semiquantitative Raman spectroscopy on single droplets for a multi-scale investigation of oil encapsulation

SEBASTIAN HÖHNE,[1,*] VANESSA ZWINGER,[1] STEFAN HEIßLER[2] and VOLKER GAUKEL[3]

[1]*Institute of Process Engineering in Life Sciences, Food Process Engineering, Karlsruhe Institute of Technology, Kaiserstraße 12, Karlsruhe 76131, Germany,* [2]*Institute of Functional Interfaces, Karlsruhe Institute of Technology, Hermann-von-Helmholtz-Platz 1, Eggenstein-Leopoldshafen 76344, Germany, and* [3]*Institute of Food Technology and Bioprocess Engineering, Max Rubner-Institut, Federal Research Institute of Nutrition and Food, Haid-und-Neu-Str. 9, Karlsruhe 76131, Germany*

Background, Context or Rationale:
Spray drying is widely used in the dairy industry to produce powders with encapsulated oil droplets. For these products, the amount of free surface oil critically determines product properties. Understanding the mechanisms leading to an excellent encapsulation of oil could help to maximise the product quality of dairy products.

Aim(s):
This study investigates the role of the locking point on the encapsulation of oil by varying oil concentration, initial drying temperature and matrix material.

Methods:
We used a multi-scale approach combining encapsulation data from single droplet drying (SDD) experiments achieved with semiquantitative Raman spectroscopy and data from spray-dried powders achieved with conventional solvent extraction.

Major Findings:
Our findings reveal that less oil is encapsulated for parameter changes leading to a later locking point. Conversely, an earlier locking point, achieved by increasing the drying temperature, significantly improves encapsulation efficiency in spray-dried powders. Substituting maltodextrin with a modified starch reveals potential influences on the morphology, with poorer encapsulation despite a shorter time to the locking point. The semiquantitative Raman measurements on SDD particles provided insights into surface composition, which correlated well with the general trend of encapsulation efficiency measured by solvent extraction in spray-dried powders.

Scientific or Industrial Implications:
This study highlights the locking point as a crucial parameter for encapsulation success and offers a powerful analytical toolbox for optimising spray-drying processes to enhance oil encapsulation in spray-dried emulsion powders.

Keywords Single droplet drying, Raman spectroscopy, Surface composition, Encapsulation, Spray drying, Multi-scale analysis.

*Author for correspondence. E-mail: s.hoehne@kit.edu

INTRODUCTION

Spray drying of emulsions is one of the most commonly used encapsulation techniques in the dairy industry (Arshady and George 1993; Gharsallaoui *et al*. 2007), as the process is well-suited to handle heat-sensitive products over a wide range of capacities (Mujumdar 2015). In these applications, feed emulsions are atomised into fine droplets, which are subsequently dried in a hot air stream (Masters 2002). One of the most important quality parameters for oil-containing powders is the amount of free surface oil of the powder particle (Vega and Roos 2006; Drusch and Berg 2008; Haas *et al*. 2019). A large amount of oil on a particle's surface can impede powder flowability and accelerate oxidation processes. Consequently, industrial products usually aim to encapsulate as much oil as possible within the solid matrix of the particles, providing protection against oxidation effects and reducing cohesiveness (Fitzpatrick *et al*. 2004). The amount of free surface oil depends largely on the formulation composition and on the drying conditions, making it crucial to gain a precise understanding of the spray droplet's drying process.

During the drying process, droplets initially heat up to the wet bulb temperature (Mujumdar 2015). After reaching this point, the droplet dries at a nearly constant rate, the droplet size decreases and a concentration gradient may form between the droplet's surface and its core (Nešić and Vodnik 1991; Abdullahi *et al*. 2020). A skin forms when a critical solute concentration is reached at the droplet's surface, marking the beginning of the falling rate period. During this period, the droplet's skin deforms, heat and mass transfer rates decrease, and droplet temperature increases. Different particle morphologies may develop during drying, depending heavily on process conditions and formulation components (Walton and Mumford 1999). For large molecules, such as hydrocolloids, the resulting dry particles usually display a hollow core with a smooth or wrinkled surface (Abdullahi *et al*. 2020; Eijkelboom *et al*. 2024a, 2024b). This morphology develops when water vapour is formed faster than it can diffuse through the porous skin, leading to the formation of vacuoles that may also cause a cycle of inflation or deflation. At very high drying rates, particles may also exhibit cracks, blow holes, or, in extreme cases, shatter into small fragments (Abdullahi *et al*. 2020).

Although the topic of encapsulation in spray drying of emulsions has been widely investigated, the impact of drying rate and particle morphology on encapsulation remains not completely understood. During the initial constant rate period, oil droplets within the spray droplet may accumulate at the droplet surface, leading to free oil on the dried particle's surface (Drusch and Berg 2008; Frascareli *et al*. 2012). This process is thought to stop once a sufficiently solid skin is formed. The latter is usually correlated with the locking point, where the drying droplet's morphology first deviates from its original spherical shape (Eijkelboom *et al*. 2024a, 2024b). After the locking point, the particle morphology develops further, and the formation of morphological features such as cracks and blow holes may also lead to an increase of free surface oil. Therefore, a comprehensive investigation of the correlations between process and formulation parameters with the locking point and the final particle morphology is necessary to gain insights into the mechanistic of the encapsulation of oil. To achieve this, single droplet drying (SDD) experiments have become more and more a focal point of spray drying research (Schutyser *et al*. 2019).

In SDD experiments, an isolated droplet is dried under a controlled drying environment to investigate drying kinetics and morphology development (Fu *et al*. 2012). Ideally, the drying temperature, air humidity and air mass flow are set to mimic the convective drying process in a spray tower. A commonly employed experimental set-up is a hanging droplet configuration, in which a single droplet is suspended on a thin filament (Wang *et al*. 2014; Malafronte *et al*. 2015; Shamaei *et al*. 2016). This allows continuous monitoring of mass and morphology of the droplet during drying (Nuzzo *et al*. 2015a). For emulsion-based systems, solvent extraction methods are traditionally employed to analyse the encapsulation of oil in spray-dried particles. In these methods, the mass of the extracted surface oil is determined gravimetrically. This is unfeasible for the application to particles from SDD, as the number and mass of particle mass and number is too low for a reliable measurement. Therefore, methods such as XPS (Nuzzo *et al*. 2015a) or Raman spectroscopy (Nuzzo *et al*. 2015a, 2015b; Eijkelboom *et al*. 2024a, 2024b) have been used to study the surface composition of particles from SDD. While these methods have provided qualitative insights into a particle's surface composition and oil coverage, they have not yet yielded more quantitative information on oil encapsulation (Eijkelboom *et al*. 2024a, 2024b).

This study aimed to investigate the impact of the locking point on oil encapsulation in spray-dried emulsions. We hypothesise that a longer time to reach the locking point leads to less encapsulated oil in the dry particle, as oil may accumulate at the surface of the drying droplet during the constant rate period (Routh and Zimmerman 2004; Shamaei *et al*. 2016). This assumption is based on the premise that particles with low diffusion coefficients, such as oil droplets, are captured by the faster receding drying front. Process and formulation parameters that are expected to influence the time to reach the locking point based were identified based on literature (Shamaei *et al*. 2016; Eijkelboom *et al*. 2023), and the following hypotheses regarding their impact on the locking point and thus encapsulation were formulated:

1 Increasing the oil-to-matrix-material ratio at a constant dry matter concentration leads to a longer time to reach the locking point and a poorer oil encapsulation, as the

solute concentration in the continuous phase of the emulsion is lower.
2 Increasing the initial drying temperature leads to an earlier locking point and an improved oil encapsulation, as the drying rate is higher.
3 Increasing the chain length of the matrix material leads to a lower diffusion coefficient and thus a faster concentration of the matrix material at the droplet's surface. This leads to an earlier locking point and thus improved encapsulation.

To investigate these hypotheses, emulsions with different oil-to-matrix-material ratios were dried with varying time–temperature histories in both SDD and spray drying. Two different emulsion systems were investigated: one containing maltodextrin and whey protein isolate (WPI), and one containing a modified starch. To ensure that particle size has no significant impact on the encapsulation of oil, the particle size was aimed to be constant in SDD and spray-drying experiments. The locking point and morphology development were monitored in SDD experiments, and the surface composition was characterised semiquantitatively using Raman spectroscopy. This semiquantitative approach showed the potential of Raman measurements in SDD. A fully quantitative study was not feasible, as the complexity of the formulation and of the processes during drying would require a large number of reference measurements that cannot be afforded in SDD. To evaluate the applicability of the SDD findings to spray drying, the encapsulation efficiency (EE) of the oil in the spray-dried powders was investigated using a standard solvent extraction method. This approach was necessary due to fundamental geometrical differences between particles from SDD and spray drying. The small size and strong surface curvature of particles from spray drying make Raman measurements unreliable for powder samples. Particles from SDD exhibit a more planar particle surface and are better suited for repeatable Raman and comparable Raman measurements. One of the main challenges for the solvent extraction method is that organic solvents can reach the interior of particles through blow holes and cracks (Kim *et al*. 2005). The washing step of the chosen solvent extraction method was therefore specifically designed to dissolve only the free surface oil of powders with maltodextrin and WPI as matrix materials (Bae and Lee 2008). The results of this study contribute to understanding the mechanisms leading to differences in surface composition and expand the toolbox for spray drying process characterisation and optimisation.

MATERIALS AND METHODS

Preparation of the model emulsions

Two model oil-in-water emulsions were investigated in this study. Both emulsions contain medium-chain triglyceride oil (MCT-oil, Witarix MCT-oil 60/40, IOI Oleo GmbH, Germany), primarily composed of C8 caprylic chains together with longer C10 chains in a 60:40 ratio respectively, as dispersed phase, but differ in the matrix material and emulsifier used. The first emulsion contains WPI (Lacprodan® DI-9224) as an emulsifier, and maltodextrin DE 14 (C*DryTM MD 01910; Cargill Deutschland GmbH, Krefeld, Germany) as a bulk matrix material. In the second model emulsion, WPI and maltodextrin are substituted with a modified starch (starch sodium octenyl succinate, C*Em-Cap; Cargill Deutschland GmbH). The chosen starch is modified for emulsification purposes, combining matrix material and emulsifier in one component. Emulsion preparation was performed in a two-step process according to the procedure described in the work of Taboada *et al*. (2021). In short, a concentrated emulsion with an oil concentration of 50 wt% is first prepared and subsequently diluted to the desired oil concentration and viscosity. For the concentrated emulsion, WPI or modified starch respectively is dissolved in water and the pH adjusted to 7.0 with a 0.5 M solution of NaOH. The ratio of emulsifier to oil was 0.1 in the concentrated emulsions and above the critical value that is needed for droplet stabilisation at stationary conditions. The MCT-oil is then added under stirring using a propeller stirrer. Subsequently, the premix is homogenised using a high-pressure homogeniser (Microfluidizer M-110EH; Microfluidics, Westwood, LA, USA) operated at 500 bar for a single pass. The Sauter mean diameter of the oil droplets in the final concentrated emulsion was around 0.29 µm, measured via laser diffraction spectroscopy (PARTICA LA-950 V2; Horiba, Tokyo, Japan). The oil droplet size was chosen to minimise oil droplet coalescence during drying, leading to measured values of oil droplet size in the spray-dried and reconstituted powder in the range of 0.23–0.3 µm for all samples, indicating no impact on encapsulation. The concentrated emulsion is in a second step diluted using maltodextrin or modified starch solution to reach oil concentrations in a range of 20 to 60 wt% (dry matter basis) to achieve different oil-to-matrix-material ratios. The total dry matter content was kept constant at 25 wt%.

Single droplet drying experiments

Drying of single droplets was conducted using a hanging-droplet experimental set-up. In this set-up, 3 µL droplets is attached to a glass filament using a 10-µL glass microliter syringe (Hamilton Company). The glass filament is in turn attached to a balance, allowing the inline monitoring of drying kinetics and drying time. Droplets are dried under dynamic temperature conditions to mimic the time–temperature histories that droplets experience during spray drying. The initial temperatures were set to 100 or 120°C with an air flow of 1.2×10^{-5} m^3/s. After deposition of the droplet on the glass filament, the air temperature was rapidly lowered to a final temperature of 65°C. A total of five

droplets were dried for each parameter combination to determine the locking point. The droplet shape is recorded during the drying process with an IDT Highspeed Os 8 digital camera (Imaging Solutions GmbH, Eningen unter Achalm, Germany) equipped with a Sigma 150 mm f/2.8 EX DG Macro lens (Sigma Corporation, Kanagawa, Japan). Images were captured at 30 frames per second for approximately 4 min and used to determine the locking point of the droplets.

To determine the final morphology of particles from single droplet drying and spray drying, scanning electron microscopy (SEM) images were taken at the Laboratory for Electron Microscopy (Karlsruhe Institute of Technology, Karlsruhe, Germany) using a LEO 1530 scanning electron microscope (Gemini Noran Instruments; Zeiss, Jena, Germany). Samples were prepared by securing the glass filaments to the sample holder with conductive silver adhesive. Subsequently, the samples were sputter-coated with a 12-nm layer of carbon at a 40° application angle (Leica AM ACE600, Leica Microsystems GmbH, Wetzlar, Germany). The images were taken with an acceleration voltage of 3 kV. One particle from SDD and one spray-dried powder sample were investigated per parameter combination.

Raman spectroscopy

To assess the encapsulation of oil in particles from SDD, the surface composition was analysed using Raman spectroscopy. Raman spectra were recorded on a Bruker Senterra 2 spectrometer (Bruker Optics, Ettlingen, Germany). For this purpose, the dried particles were mounted on a gold mirror and placed in the excitation laser focus. A square of 25 × 25 µm was measured at 10 different positions on each droplet, as shown in Figure 1. Raman measurements were carried out at room temperature using a diode laser, with a wavelength of $\lambda = 785$ nm, operated at 50 mW power. An Olympus LMPLFLN 20× Objective (Olympus K.K., Tokyo, Japan), with a numerical aperture of 0.4, was used for observation of the sample, focussing the excitation beam and collimating the backscattered light. Each spectrum was integrated over 20 s with 4 coadditions (5 s per coaddition). To obtain a single spectrum for a parameter combination, the spectra from 10 different positions on three distinct particles for a total of 30 spectra were averaged. As spectra are mainly used for qualitative investigations, standard deviations are omitted from the graphical representation of the spectra to prevent visual clutter. Data processing was performed with Bruker OPUS software Ver. 8.1; baseline correction was applied using the concave rubber band method. Spectra were normalised using vector normalisation based on the file limits of the spectra.

As a reference, the Raman spectra of the pure components were obtained using 100 coadditions with 5-s integration time per coaddition. The averaged results are shown in Figure 2. Based on the determined spectra, specific Raman bands were identified that are unique to the spectrum of the respective component. The Raman band for MCT-oil was found to be 1744 cm^{-1} related to the C=O symmetrical stretching band, corresponding well with literature (Kwofie *et al*. 2020; Esmonde-White *et al*. 2022). For the matrix materials maltodextrin and modified starch, the characteristic Raman band of 480 cm^{-1} was identified, which is observed in the skeletal-mode region and a typical marker of starch and its derivatives (Rodrigues Júnior *et al*. 2016; Farahi *et al*. 2020). The Raman band for WPI was identified via the amide I region at a wavenumber of 1665 cm^{-1} (Zhang *et al*. 2012). To obtain semiquantitative results using Raman spectroscopy, data are evaluated based on the height of characteristic Raman bands, which are compared to an ideal, homogeneous distribution of the components. The peak heights are averaged across all 30 individual spectra per parameter combination, and the standard deviation is calculated.

Spray drying experiments

A pilot-scale single-stage co-current spray dryer (Werco SD20, Hans G. Werner Industrietechnik GmbH, Reutlingen,

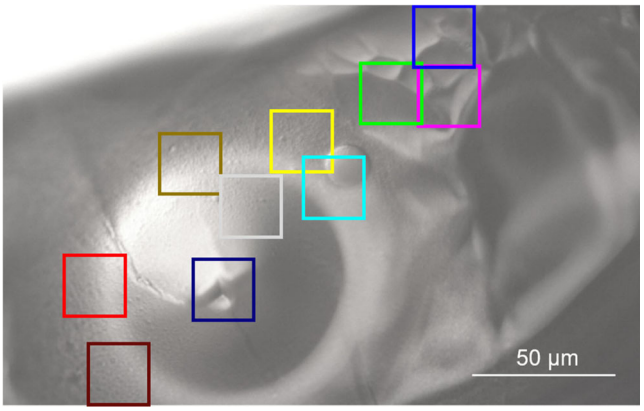

Figure 1 Image of a particle's surface taken with a confocal Raman microscope. The coloured boxes indicate the measurement areas that were selected to generate the Raman spectra. Particle dried at $T_{Start} = 100°C$, $T_{End} = 65°C$ and $c_{Oil} = 20$ wt%.

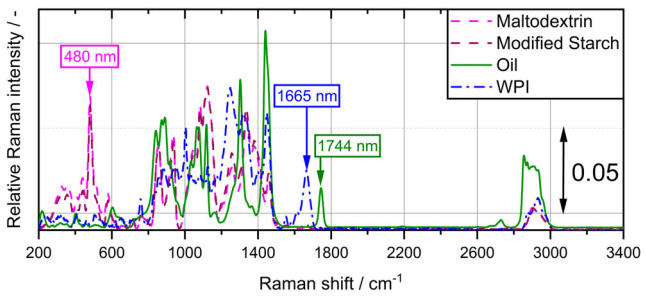

Figure 2 Raman spectra for the pure components of the model emulsions.

Table 1 Overview of the investigated parameter combinations in the spray drying trials. MD denotes that a combination was used to dry the maltodextrin-based system, while MS marks the starch-based system.

	Spray drying		
Oil concentration	180°C	200°C	220°C
20 wt%	MD, MS	MD	MD, MS
40 wt%	MD, MS	MD	MD, MS
60 wt%	MD, MS	MD	MD, MS

Germany) was used for spray drying trials. The feed emulsion was supplied to the spray dryer for atomisation with a three-piston pump (Rannie LAB Typ 8.5, SPX FLOW Inc., Charlotte, NC, USA). Atomisation was performed using a pressure-swirl nozzle (SKHN-MFP SprayDry, Spraying Systems Co., Glendale Heights, IL, USA) at a pressure of 50 bar with the feed emulsion at room temperature. Inlet air temperatures of 180, 200 and 220°C were investigated. For an outlet air temperature of 85°C, the air flow rate was set between 600 and 800 m^3/h. A comprehensive overview of the spray-dried powders is given in Table 1. The powder samples were collected with a sample container and subsequently stored at room temperature in airtight containers for powder analysis. Agglomeration was not enforced in the process by any means.

The encapsulation of oil in the spray-dried samples was measured with a commonly used solvent extraction method. Based on the results of the extraction, the encapsulation efficiency (EE) is calculated, which is the ratio of oil encapsulated within the particle to the total mass of oil in the powder sample (Eqn 1). In this study, the employed solvent extraction method is based on literature (Tan *et al*. 2005; Bae and Lee 2008) with the exception that a rotary evaporator was used for evaporation of the solvent instead of a fume hood. In the first step, 1.5 g of powder was weighed into a rolled rim glass and 15 mL of n-hexane (≥ 95%, Carl Roth GmbH & Co. KG, Karlsruhe, Germany) were added. The suspension was shaken for 2 min on a vortex mixer. Subsequently, the n-hexane was removed from the powder sample by vacuum filtration using filter paper with a pore size of 2.5 µm (Whatman No. 5; Cytiva, Pensacola, FL, USA). The powder sample was then washed with an additional 15 mL n-hexane and transferred to a round bottom flask. A rotary evaporator (Laborota 4000 efficient, Heidolph Instruments GmbH & Co. KG, Schwabach, Germany) was used at 150 mPa to separate the solvent. The round bottom flask was kept in a 50°C water bath at a rotation speed of 30 rpm until the n-hexane was completely evaporated. The EE is calculated according to the following equation:

$$\mathrm{EE} = \frac{m_{\mathrm{oil},T} - m_{\mathrm{oil},E}}{m_{\mathrm{oil},T}} \quad (1)$$

with $m_{\mathrm{oil},T}$ being the total oil mass in the powder sample, and $m_{\mathrm{oil},E}$ the mass of extracted oil. To minimise the impact of powder particles potentially breaking through the filter paper, or the solvent partially dissolving the matrix material, a blank value was determined using a sample containing no oil. All measurements were conducted in triplicate.

Residual moisture was determined gravimetrically. For this, 1.5 g of powder was added to aluminium test pans and dried at 100°C in a drying cabinet (Trockenofen T 6060, Heraeus Instruments GmbH, Hanau, Germany) until an equilibrium was reached. Before final weighing, the samples were stored in a desiccator for 2 h and the residual moisture RM was then determined according to Eqn 2:

$$\mathrm{RM} = \frac{m_0 - m_D}{m_0} \quad (2)$$

with m_0 being the mass of the powder sample before drying and m_D the mass after drying. The residual moisture was determined in triplicate for each sample and used to determine the total oil mass in a given powder sample for the calculation of the EE.

As the size of the powder particles may have an influence on the encapsulation in spray dried powders, the particle size was determined using a LS 13320 Beckman Coulter laser diffraction spectroscope (Beckman Coulter, Brea, CA, USA). The measurements were conducted in triplicate with a refractive index for maltodextrin of 1.53. Sauter mean diameter and $x_{10,3}$-values of the distributions were measured, indicating no significant impact on encapsulation efficiency (Linke *et al*. 2020). A complete overview of the Sauter mean diameters and $x_{10,3}$-values of the particle size distributions is included in Appendix A.

Statistical analysis

Statistical analysis was conducted using OriginPro 2023. The data of the time until the locking point is reached and the drying time are presented as the mean standard deviation from all measurements. To determine whether there are significant differences in these results, a one-way ANOVA with a Tukey's test was performed. Furthermore, homogeneity of variance was confirmed for all data sets using a Brown–Forsythe test. A significance level of $P < 0.05$ was used for all analyses.

RESULTS AND DISCUSSION

This study aimed to explore the effect of the locking point on the encapsulation of oil in spray dried powders. For this, process and formulation parameters influencing the time to reach the locking point were identified and systematically

investigated. SDD and spray-drying experiments were conducted and the encapsulation compared. The impact of the oil concentration and starting temperature on the oil encapsulation is shown in the first section, comparing the morphology development and drying time to reveal potential correlations between these parameters and the encapsulation of oil. Thereafter, the results for the Raman spectra are presented and discussed, before the encapsulation of particles from SDD and spray drying is compared. For this purpose, the peak heights of the Raman spectra were used to analyse the surface composition and encapsulation for SDD particles. For spray-dried samples, however, a solvent extraction method was used to measure encapsulation efficiency, as Raman measurements are not feasible for spray-dried samples. The second section focusses on the influence of a matrix material change, comparing the maltodextrin model system with a system containing a modified starch. Again, results for the morphology development and drying time are presented first, before the encapsulation is discussed.

Impact of oil concentration and starting temperature on encapsulation, morphology development and drying time of single droplets

SDD experiments were conducted for emulsions with different oil concentrations. The time to reach the locking point and the drying time were investigated, and the results are shown in Table 2. The results reveal an increase in the time to reach the locking point t_{LP} with increasing oil concentration at constant dry matter concentration. This aligns well with findings reported in the literature (Shamaei *et al*. 2016). The observed trend is expected, as a lower matrix material concentration in the continuous phase prolongs the time required until a sufficiently high solute concentration for skin formation and surface deformation. According to the general hypothesis, this result suggests a lower oil encapsulation for higher oil concentrations for particles from SDD and spray drying.

Looking at the drying time, a trend is discernible for a decrease in drying time for an increasing oil concentration. However, it is only significant comparing 20 and 60% oil. This finding is likely due to two factors. First, a longer time to reach the locking point means that the constant rate period is also longer, sustaining the highest drying rate period longer. Second, the formation of morphological features such as blow holes or cracks could lead to a lower mass transfer resistance for water vapour being transported through the porous dried matrix.

Looking at the results for varying starting temperatures T_{start}, it is anticipated that both the time to reach the locking point and drying time are shorter for higher T_{start} when drying droplets at a constant oil concentration (Shamaei *et al*. 2016). The results displayed in Table 3 confirm both expectations. According to the general hypothesis, it is assumed that the shorter time to reach the locking point leads to less free surface oil. While the shorter drying time is not expected to have an influence on the encapsulation per se, it could affect the final particle morphology, which may in turn influence the encapsulation. Previous studies have connected a higher temperature with a higher amount of cracked or fractured particles (Walton and Mumford 1999). This shows the necessity to consider the final particle morphology to evaluate a possible superposition of process and formulation parameters with morphology development.

SEM images were taken of one particle per parameter combination, with exemplary pictures shown in Figure 3. The presented particles were generally spherical, with a smooth, cracked surface. While some particles displayed some small wrinkles (Figure 3b, d, f) and some particles had more smooth surfaces (Figure 3a, c, e), the SEM images show no clear correlation between the particle morphology and the initial temperature. As a notable difference, a blow hole is observed for an oil concentration of 60 wt% and 100°C, but not for 120°C. Blow holes are usually expected to be favoured for parameter combinations that lead to higher drying rates and an earlier locking point. Interestingly, the blow hole was observed for the particle that had the latest locking point and longest drying time. This indicates that blow holes could perceivably develop for

Table 2 Time until the locking point is reached and drying time for particles with different oil concentrations.

Oil concentration	Time until Locking point is reached	Drying time
20 wt%	35.0 ± 2.2 s^{A}	119.3 ± 21.3 s^{a}
40 wt%	41.1 ± 4.9 s^{A}	110.6 ± 17.3 s^{ab}
60 wt%	47.6 ± 3.7 s^{B}	96.3 ± 14.0 s^{b}

Particles were dried at $T_{start} = 100$°C and $T_{end} = 65$°C. Superscript letters indicate significant differences based on a one-way ANOVA with a Tukey's test. Values within the same column sharing a common letter are not statistically different ($P > 0.05$).

Table 3 Time until the locking point is reached and drying time for particles with start temperatures.

T_{start}	Time until locking point is reached	Drying time
100°C	41.1 ± 4.9 s^{A}	110.6 ± 17.3 s^{a}
120°C	21.9 ± 6.7 s^{B}	75.8 ± 11.9 s^{b}

Particles with an oil concentration of 40 wt% were dried at $T_{end} = 65$°C. Superscript letters indicate significant differences based on a one-way ANOVA with a Tukey's test. Values within the same column sharing a common letter are not statistically different ($P > 0.05$).

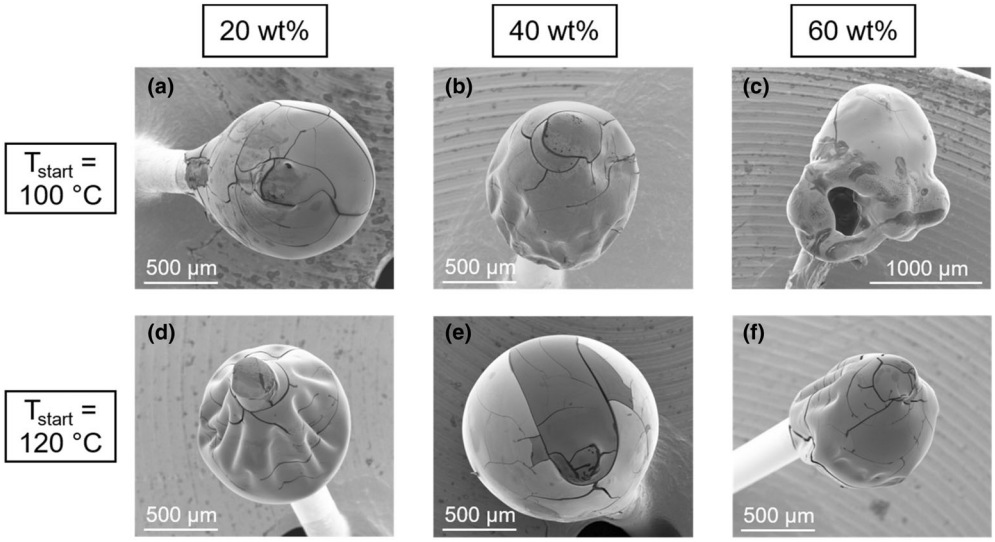

Figure 3 SEM micrographs of SDD particles dried at different $T_{start} = 100°C$ (a–c) and 120°C (d–f) for oil concentrations of 20 wt% (a and d), 40 wt% (b and e), and 60 wt% (c and f). T_{end} was kept constant at 65°C (SEM images acquired by the Electron Microscopy Laboratory at the Karlsruhe Institute of Technology).

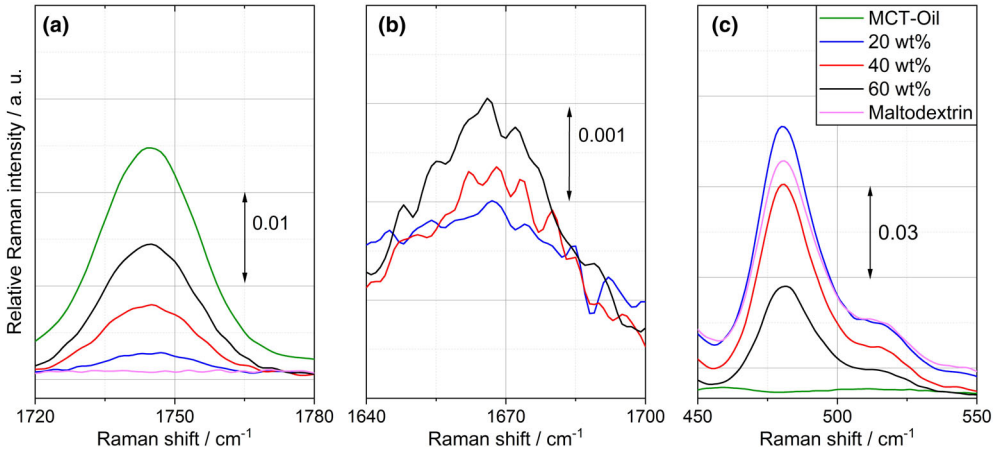

Figure 4 Characteristic bands of the Raman spectra for MCT-oil (a), WPI (b) and Maltodextrin (c) for particles dried with different oil concentrations. Particles were dried at $T_{start} = 100°C$ and $T_{end} = 65°C$. The shown spectra represent the average of all measured spectra per parameter combination.

all investigated temperature combinations and oil concentrations, although it may not be captured in these exemplary images of one of the five droplets per parameter combination. Furthermore, no clear impact of the oil concentration on the morphology can be discerned, a finding that is consistent with studies from Both *et al*. (2018) and Eijkelboom *et al*. (2024a, 2024b). The results of Figure 3 thus lead to the assumption that the morphology development has no major influence on oil encapsulation during these trials.

Investigation of the surface composition of single droplets using Raman spectroscopy

Raman spectroscopy was used to investigate the surface composition of the particles from SDD experiments. Figure 4 shows the characteristic bands of the Raman spectra for each component of the model system across oil concentrations from 20 to 60 wt%. Drying temperatures were $T_{Start} = 100°C$ and $T_{End} = 65°C$. For MCT-oil (Figure 4a), the results show that oil is detected on the surface of particles for all compositions, as confirmed by the characteristic C=O symmetrical stretching band leading to a peak at 1744 cm^{-1}. As expected, the peak of the relative Raman intensity increases with increasing oil content. The spectra of pure MCT-oil were measured for comparison, exhibiting the strongest intensity for all samples. Based on these results, it is expected that the relative Raman intensity of WPI also increases with increasing oil content, given that WPI is adsorbed at the surface of the oil droplets, and

should thus also accumulate at the particle surface. This trend is overall confirmed by the results shown in Figure 4 (b). An increase in intensity from 60 wt% to 20 wt% is observed. It should be noted, however, that no obvious difference between samples containing 20 and 40 wt% oil can be concluded, which is due to the relatively high measurement noise at this low WPI concentration. Finally, if both MCT-oil and WPI show higher Raman intensities for higher oil concentrations, the presence of maltodextrin at the surface is anticipated to decrease, a result that is evident in Figure 4(c). Interestingly, the relative Raman intensity for an oil concentration of 20 wt% was higher than for the pure component spectrum. This discrepancy is likely caused by the difference in particle size scale, with particles from SDD being much larger than the maltodextrin powder particles. The different curvatures of the particles lead to differences in the relative Raman intensities of the samples, as the scattering of the Raman signal is intrinsically surface-dependent.

Overall, similar results were obtained for $T_{start} = 120°C$ (Appendix B), with one key difference for the 20 and 40 wt % oil concentration spectra. The results show a higher Raman intensity for the Raman band of oil at 20 wt% compared to 40 wt%, while the maltodextrin band shows a lower Raman intensity at 20 wt% compared to 40 wt%. To properly assess the cause of this discrepancy between the results at $T_{Start} = 100°C$ and 120°C, the variance of the measurement and between each particle needs to be considered, which will be done in the following section (Figure 5).

While the data presented in Figure 4 successfully describe differences in the surface composition of particles for a given parameter combination, it does not allow for direct conclusions about the oil encapsulation. This is because it only gives a qualitative indication of an increase of surface oil with an increase of the oil concentration, without correlating it to the total oil in the particle. To address this, the height of the characteristic Raman band of oil is evaluated in the following section, with the results compared to the EE of spray-dried powders.

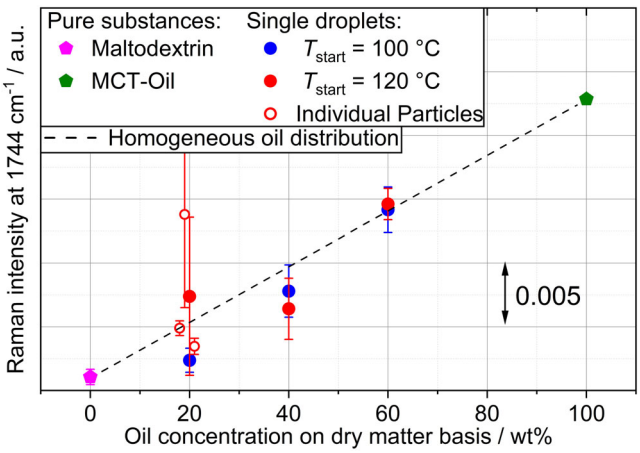

Figure 5 Peak height of the characteristic band of the Raman spectrum for MCT-oil at a wave number of 1744 cm^{-1} over the oil concentration for the pure components of maltodextrin (0 wt% oil) and MCT-oil (100 wt% oil), and for particles from single droplet drying with oil concentrations from 20 to 60 wt%. The particles were dried at $T_{end} = 65°C$.

Comparison of the oil encapsulation of SDD particles and spray dried powders

Figure 5 shows the height of the peak of the characteristic Raman band of MCT-oil over the oil concentration. For this, the relative Raman intensity at a wave number of 1744 cm^{-1} is shown, which is the characteristic band of the MCT-oil spectrum. The Raman intensities are shown for SDD samples with oil concentrations from 20 to 60 wt%, dried at T_{start} of 100 and 120°C. The peak heights of the pure component spectra from maltodextrin and MCT-oil are included as reference values. As a visual guide, these two data points are connected by a dashed line, marking the Raman intensities for a homogeneous distribution of the components over the oil concentration. Intensities measured at the particles' surface above the dashed line suggest more oil on the surface and thus a poor encapsulation, while values below indicate less surface oil and an improved encapsulation.

Taking a look at the results for a temperature of $T_{start} = 100°C$, the Raman intensity increases with increasing oil concentration, as shown in Figure 4(a). Comparing the data with the homogeneous distribution reference line, the intensity for samples with 20 wt% oil is around 60% lower than the homogeneous distribution indicated by the dashed line. As the oil concentration is increased to 40 wt%, the Raman intensity shows a stronger increase relative to the reference line. This trend continues for a further increase to 60 wt%, where the measurement values are only 2% lower than the theoretical value, indicating a poorer encapsulation with increasing oil concentration. The calculation of the distance of the measured Raman intensity from a homogeneous distribution is described in Appendix C. This observed trend fits well with the expectation based on the locking point behaviour shown in Table 2, which indicated a delayed locking point at higher oil concentrations. When considering the impact of different temperatures, it was shown previously that the locking point is reached earlier for the higher temperature of $T_{start} = 120°C$ compared to 100°C. It is consequently expected that more oil is encapsulated for $T_{start} = 120°C$, leading to lower Raman intensities. However, the experimental results show overall no clear difference in Raman intensities between the two temperatures. Both temperatures yielded similar Raman intensities at oil concentrations of 40 and 60 wt%. Larger Raman intensities were only observed for an oil concentration of 20 wt% and $T_{start} = 120°C$, for which the standard deviation is also noticeably larger. To investigate whether this was due to a single outlier, the Raman intensities for the three individual

particles are compared. The comparison reveals that one particle had a significantly higher Raman intensity than the others. While the exact reason is not clear, a possible explanation is related to the morphology of the particles. As shown in the SEM images in Figure 3, morphological features such as surface damages by blow holes can be observed in some cases, which could lead to additional surface oil. This local phenomenon could also explain the larger standard deviation that is observed for this particular particle, as the oil content on the surface would be less homogeneous.

To further elucidate this and compare the results from SDD to the spray-drying process, the EE was investigated for spray-dried powders. Based on the results from SDD, it is expected that the EE of spray dried powders decreases with increasing oil concentration, while the drying temperature has no clear impact.

The results of the EE of spray-dried powders with oil concentrations from 20 to 60 wt% are depicted in Figure 6 for T_{air} ranging from 180 to 220°C. The results reveal a decrease in the EE with increasing oil concentration for both investigated temperatures, an observation that is consistent with the expectation from the SDD measurements. Looking at the impact of the drying temperature, the EE increases with increasing T_{in} from 180 to 200°C for all investigated oil concentrations. While this observation is in contrast to the expectation based on SDD, it aligns well with the initial hypothesis and literature results (Höhne and Gaukel 2024). However, a further increase of the inlet air temperature to 220°C leads to a plateauing of the EE, showing a result that is similar to the results of SDD. One explanation could lie in morphological differences of the powders spray-dried at different temperatures, yet no significant variations in the particle morphology were observed in SEM images of the spray-dried particles (Appendix D). This suggests that the plateauing of the EE is not correlated with particle morphology, but rather that the drying rate at $T_{in} = 200$°C is high enough to prevent a redistribution of oil towards the droplet surface during drying. In this case, an additional increase in drying rate does not lead to an increase in EE.

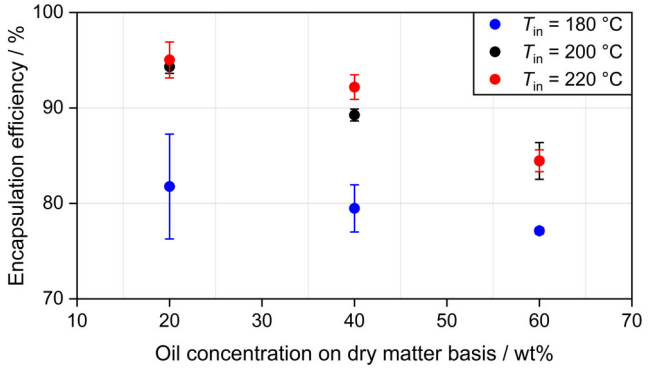

Figure 6 Encapsulation efficiency over the oil content for spray dried powders at different inlet temperatures and constant outlet temperature $T_{out} = 85$°C and atomisation pressure of $\Delta p = 50$ bar.

As there was no impact of T_{start} on the surface composition in SDD, it is assumed that the investigated SDD particles are dried in a similar plateau region, where encapsulation is relatively independent from the drying temperature, despite the much lower drying temperatures in SDD than in spray drying. A possible explanation could lie in the particle size when the locking point is reached, which is likely quite similar for both SDD temperatures, leading to a similar amount of oil accumulating at the receding droplet surface. Furthermore, the difference in droplet size needs to be accounted for. While droplets from SDD are around 1.2 mm in diameter, the size of spray-dried starch particles is around 40 µm. A change in drying air temperature of 20°C could thus have a significantly different impact on the ratio of the receding drying front velocity compared to the total droplet size between the two drying processes. This ratio could be less affected by the air temperature in SDD, leading to a reduced impact of the drying rate in SDD compared to spray drying. On the other hand, changes in the composition directly impact the amount of oil captured at the drying front during drying, leading to the observed differences depending on the oil concentration.

Nonetheless, the results of the spray-dried samples hint towards a potential impact of the air temperature on particle morphology, a finding that is confirmed by literature results (Eijkelboom *et al*. 2024a, 2024b), where it was shown that different temperatures may significantly impact the final particle morphology also in SDD. As this could in turn affect encapsulation, extending the range of investigated temperatures in SDD could give valuable insights into the impact of the drying temperature on the morphology and encapsulation.

Impact of matrix material on encapsulation

This section aims to elucidate the impact of the matrix material on the surface composition and encapsulation in SDD and spray drying. For this purpose, maltodextrin and WPI were substituted by an emulsifying modified starch. It was hypothesised that the starch leads to a shorter time to reach the locking point and therefore less surface oil, as starch is a larger molecule with a lower diffusion coefficient compared with maltodextrin. This leads to a faster accumulation of the starch at the droplet surface and thus a shorter time until a critical solute concentration is reached.

Morphology development and drying time of single droplets

The SDD results for the time to reach the locking point t_{LP} and the drying time of emulsions containing modified starch are depicted in Table 4. Different oil concentrations were investigated for a drying temperature of $T_{start} = 100$°C and

$T_{end} = 65°C$. Measurements at $T_{start} = 120°C$ were omitted, as the observed impact of a temperature change on the encapsulation is expected to be similar between maltodextrin and modified starch. Similar to the result for emulsions with maltodextrin (Table 2), t_{LP} increases with increasing oil concentrations, as the solute concentration in the continuous phase decreases. This leads to a longer time until a critical solute concentration at the droplet surface, and thus the locking point, is reached. Comparing the values for modified starch with the values of the maltodextrin system at the same temperature (Table 2), it can be seen that t_{LP} is reached earlier for all investigated oil concentrations for modified starch. This result is in line with the hypothesis that the locking point time is reached earlier for modified starch and that the encapsulation should be consequently higher for modified starch than for the maltodextrin system. For the results of the drying time, the modified starch emulsions showed a numerical increase from 108.7 s for 20 wt% oil to 123.9 s at 60 wt% oil, although this trend is not statistically significant. Therefore, no clear impact of the oil concentration is observed for the drying time for the modified starch systems. Overall, the values are in a similar range as those containing maltodextrin, which showed values between 119.3 s at 20 wt% oil and 96.3 s at 60 wt% (Table 2). This indicates that while the choice of matrix material influences t_{LP}, the overall energy input from the air into the droplet remains quite similar, leading to no discernible impact on the drying time.

Table 4 Time until the Locking point is reached and drying time for particles containing modified starch and different oil concentrations.

Oil concentration	Time until Locking point is reached	Drying time
20 wt%	15.8 ± 2.4 s^{A}	108.7 ± 19.9 s^{a}
40 wt%	29.0 ± 3.8 s^{B}	114.3 ± 8.4 s^{a}
60 wt%	33.5 ± 4.8 s^{B}	123.9 ± 15.1 s^{a}

Particles were dried at $T_{start} = 100°C$ and $T_{end} = 65°C$. Superscript letters indicate significant differences based on a one-way ANOVA with a Tukey's test. Values within the same column sharing a common letter are not statistically different ($P > 0.05$).

Figure 7 presents the SEM micrographs for SDD particles containing modified starch across all investigated oil concentrations. At 20 wt% oil (Figure 7a), the particle surface is wrinkled with large indentations. Compared with particles containing maltodextrin and WPI, the modified starch particles are more wrinkled, which is likely connected to the viscoelastic properties of the skin. It is reported in the literature (Both *et al*. 2020) that maltodextrin-based particles tend to form skins that are in a rubbery state and lead to more wrinkled particles. Materials that display an earlier structural arrest, such as modified starch, lead to smoother particles. The particle containing 40 wt% oil (Figure 7b) showed no major morphological difference from 20 wt% particles (Figure 7a); however, a further increase of the oil concentration to 60 wt% (Figure 7c) shows a more spherical particle with softer, less pronounced wrinkles. This can be seen as the wrinkles, defined as the folds between the indentations, become wider for 60 wt% oil. While a definitive trend cannot be established solely based on these individual particles, the influence of the oil concentration on the particle morphology is also reflected in spray-dried starch-based particles shown in Appendix E. Specifically, spray-dried particles containing 20 and 40 wt% oil showed a more wrinkled surface (Appendix E, a and b), while 60 wt% oil concentration generally leads to softer wrinkles with smaller indentations (Appendix E, c). The observed changes in particle morphology are in contrast to the observation based on the SEM images of maltodextrin particles (SDD in Figure 3 and spray drying in Appendix D), where oil concentration did not influence particle morphology. Another notable difference between modified starch particles and maltodextrin particles is the almost complete absence of cracks in the structure of starch-based particles. This observation hints

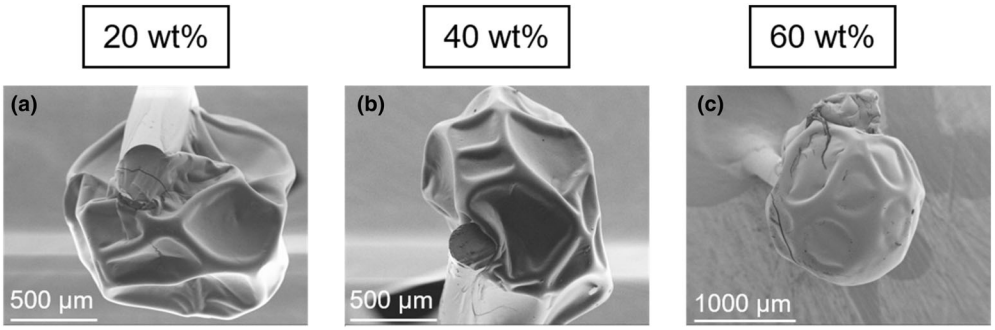

Figure 7 SEM micrographs of SDD particles containing modified starch and 20 wt% (a), 40 wt% (b) and 60 wt% (c) MCT-oil. Drying temperatures were kept constant at $T_{start} = 100°C$ and $T_{end} = 65°C$ (SEM images acquired by the Electron Microscopy Laboratory at the Karlsruhe Institute of Technology).

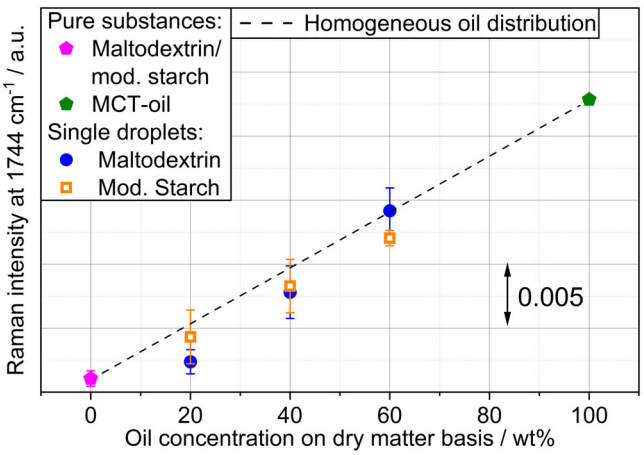

Figure 8 Relative Raman intensity at 1744 cm^{-1} over the oil concentration for the pure components of maltodextrin and MCT-oil and for particles from single droplet drying with different oil concentrations and dried at $T_{start} = 100°C$ and $T_{end} = 65°C$.

towards improved encapsulation of oil for the starch-containing system in comparison with the maltodextrin system.

Comparison of the encapsulation of oil in SDD particles and spray dried powders

Figure 8 shows the Raman intensity of the characteristic Raman band at 1744 cm^{-1}, plotted against the oil concentration on dry matter basis. Results for both modified starch and maltodextrin are shown for comparison. For more detail on the spectra of the starch-based particles, the characteristic bands are provided in Appendix F for all components. Based on the spectra, similar trends are observed for the starch-based system compared with the model system containing maltodextrin (Figure 4), as an increase in the oil concentration in the particle leads to more oil and less modified starch on the surface of the particles. Therefore, the discussion focuses directly on the results of the Raman intensity at a wave number of 1744 cm^{-1} for particles containing different matrix materials to gain more insight into the oil encapsulation.

For modified starch particles, an increase in the Raman intensity with increasing oil concentration is observed in Figure 8, which is qualitatively comparable to the maltodextrin particles. Similar to the results for maltodextrin particles, the Raman intensity values consistently remain below the dashed reference line representing a homogeneous distribution of the oil and are overall in a similar order of magnitude considering the standard deviations. When investigating the distance of the measured values to the dashed reference line, it is revealed that the Raman intensity for 20 wt% oil is 27% below the value for a homogeneous distribution of the oil, while it is only 16% below the theoretical value for 60 wt% oil concentration. The higher relative

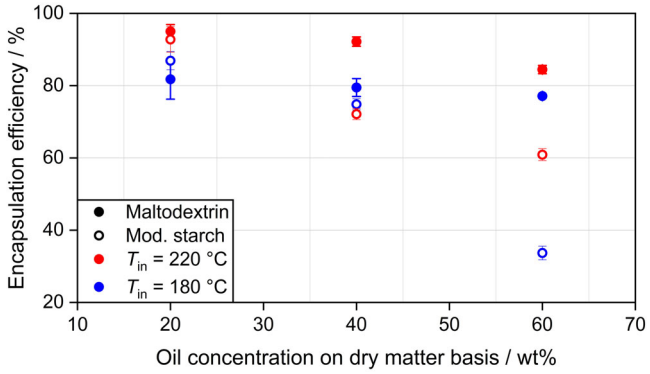

Figure 9 Encapsulation efficiency over the oil content for spray dried powders with different oil contents and inlet temperatures and constant outlet temperature $T_{out} = 85°C$ and atomisation pressure $\Delta p = 50$ bar.

distance indicates that the encapsulation is highest at the lowest oil concentration, with poorer encapsulation for higher oil concentrations. Although this trend is similar to the maltodextrin-based particles, it is much more pronounced for the maltodextrin system, which showed a substantial decrease from 60% below the homogeneous distribution value to around 2%. Based on the results from SDD, it is expected that the values of EE are in a similar order of magnitude for both model systems and that the EE decreases less with increasing oil concentration for modified starch particles.

Figure 9 depicts the EE of spray-dried powders containing modified starch together with the results of the maltodextrin samples. As expected based on the results of the time to the locking point (Table 4) and the Raman measurement (Figure 8), the EE decreases with increasing oil concentration for the modified starch system, dropping from around 92% at the lowest oil concentration to around 61% at the highest oil concentration and $T_{in} = 220°C$. Although the overall trend is comparable, the individual results from the EE are not consistent with the results from the Raman measurements. At a low oil concentration of 20 wt%, the EE for maltodextrin and the starch particles are comparable. However, the decrease in the EE with increasing oil concentrations is much more pronounced in the modified starch system, leading to a low EE of 61% at 60 wt% oil in starch-based particles compared to a much higher EE of around 84% for maltodextrin-based particles. The lower EE for modified starch compared with maltodextrin, despite the difference in locking point observed in SDD, could indicate a significant impact of the morphology. Long-chain polysaccharides, such as modified starch, are known to transition to a glassy state much more rapidly during drying compared to molecules with a lower molecular weight. This has been connected with the formation of more porous structures and surface cracks during drying, which might lead to increased free oil (Werner *et al.* 2007; Kurtz *et al.* 2025). Similar trends were observed for modified starch for $T_{in} = 180°C$. Based on the Raman spectroscopy results, it

was expected that the EE in the starch system would not be greatly influenced by the oil concentration, resulting in poorer encapsulation of oil at low oil concentrations and improved encapsulation at high concentrations compared to the maltodextrin system (Figure 8). This discrepancy between the Raman measurement of single droplets and the EE measurements from a spray-dried bulk powder could be related to morphological changes that are not fully replicated when drying a single droplet. For instance, while starch-based particles produced by SDD showed no blow holes (Figure 7), the spray-dried samples revealed blow holes in a number of particles (Appendix E). A further consideration is the difference in measurement method of the free surface oil. While Raman only measures surface oil, a solvent extraction may penetrate into the interior of the particle. Although the extraction method used in this study was developed to remove only surface oil, it was designed for a system containing maltodextrin and WPI. Since modified starch possesses different chemical and surface properties, the solvent extraction method might not be entirely compatible with the starch-based system. In general, it has to be noted that the small sample size in SDD, compared to the larger scale of spray drying, could lead to a skewed representation of the data. Further investigation is needed to confirm that the observed morphological differences between SDD and spray drying are caused by the drying method and are not a statistical anomaly attributed to the limited sample size. Nevertheless, the results for the EE in spray-dried powder highlight that drying conditions in the spray dryer can significantly alter particle morphology, and thus oil encapsulation, which may not be fully captured by SDD set-ups. Therefore, careful consideration of the drying conditions and resulting particle morphologies is crucial when transferring insights gained from SDD to the complex spray-drying process.

CONCLUSIONS

This study investigated the role of the locking point on oil encapsulation in emulsion spray drying, providing a semi-quantitative approach using Raman spectroscopy on particles from single droplet drying (SDD) experiments. Our findings confirm the central hypothesis that the time until the locking point is reached influences encapsulation efficiency, with a longer time leading to less encapsulated oil in spray dried powders.

To investigate this subject, process and formulation parameters influencing the time to reach the locking point were identified and varied, and their impact on the locking point was investigated, as well as the subsequent encapsulation of the oil. Specifically, a higher oil concentration at constant dry matter concentration was shown to delay the locking point, resulting in a poorer encapsulation for both SDD and spray-dried powders. This was quantitatively confirmed in spray-drying experiments by a decrease in encapsulation efficiency (EE) at increasing oil concentrations from 20 to 60 wt%. Similarly, a higher initial drying temperature led to an earlier locking point and shorter drying times in SDD experiments, which is reflected in higher EE in spray drying trials. This trend for the oil encapsulation was not observed in SDD.

Furthermore, substituting maltodextrin with a modified starch resulted in a shorter time to reach the locking point. While this supports the hypothesis that larger molecules with lower diffusion coefficients accumulate faster at the droplet surface, the second part of the hypothesis, that the earlier skin formation leads to a more efficient encapsulation of the oil, was not supported by the results in SDD and spray drying.

The results from SDD experiments and the semiquantitative Raman analysis were successfully correlated with the EE of spray-dried powders for the general trends. In detail, the analysis by Raman and EE showed discrepancies, which may be attributed either to different particle morphologies in spray drying compared to SDD or they are based on statistical limitations due to the small sample size in SDD. Nevertheless, this multi-scale approach provides a robust method for investigating the complex drying phenomena occurring in spray drying. Furthermore, it demonstrates that the locking point is a critical parameter for predicting and optimising oil encapsulation, connecting results from SDD to spray drying. Our findings contribute to an improved understanding of the mechanisms governing the encapsulation of oil and expand the toolbox for studying spray drying of emulsion processes.

AUTHOR CONTRIBUTIONS

Stefan Heißler: Formal analysis; investigation; methodology; writing – review and editing. **Vanessa Zwinger:** Formal analysis; investigation; methodology; writing – review and editing. **Sebastian Höhne:** Conceptualization; investigation; writing – original draft; methodology; formal analysis. **Volker Gaukel:** Conceptualization; project administration; resources; supervision; writing – review and editing.

ACKNOWLEDGEMENTS

This IGF project of the GVT was supported via AiF within the program for promoting the Industrial Collective Research (IGF) of the German Ministry of Economic Affairs and Energy (BMWi), based on a resolution of the German Parliament. Project 21662N. The authors express their gratitude to Markus Fischer, Jonas Kaltenbach, Volker Zibat and Christoph Egli for the experimental support. Open Access funding enabled and organized by Projekt DEAL.

CONFLICT OF INTEREST STATEMENT

The authors declare no conflicts of interest.

DATA AVAILABILITY STATEMENT

The data that support the findings of this study are available from the corresponding author upon reasonable request.

REFERENCES

Abdullahi H, Burcham C L and Vetter T (2020) A mechanistic model to predict droplet drying history and particle shell formation in multi-component systems. *Chemical Engineering Science* **224** 115713.

Arshady R and George M H (1993) Suspension, dispersion, and interfacial polycondensation: A methodological survey. *Polymer Engineering & Science* **33** 865–876.

Bae E K and Lee S J (2008) Microencapsulation of avocado oil by spray drying using whey protein and maltodextrin. *Journal of Microencapsulation* **25** 549–560.

Both E M, Karlina A M, Boom R M and Schutyser M A I (2018) Morphology development during sessile single droplet drying of mixed maltodextrin and whey protein solutions. *Food Hydrocolloids* **75** 202–210.

Both E M, Tersteeg S M B, Boom R M and Schutyser M A I (2020) Drying kinetics and viscoelastic properties of concentrated thin films as a model system for spray drying. *Colloids and Surfaces A: Physicochemical and Engineering Aspects* **585** 124075.

Drusch S and Berg S (2008) Extractable oil in microcapsules prepared by spray-drying: Localisation, determination and impact on oxidative stability. *Food Chemistry* **109** 17–24.

Eijkelboom N M, Swinkels A C M, de Ruiter J, Boom R M, Wilms P F C and Schutyser M A I (2023) High-resolution thermography and modelling allows for improved characterization of drying sessile single droplets. *Journal of Food Engineering* **341** 111340.

Eijkelboom N M, Gawronska K, Vollenbroek J M, Kraaijveld G J C, Boom R M, Wilms P F C and Schutyser M A I (2024a) Single droplet drying with stepwise changing temperature-time trajectories: Influence on heat sensitive constituents. *Food Research International* **182** 114194.

Eijkelboom N M, Hooiveld E, Kingma J, Boom R M, Wilms P F C and Schutyser M A I (2024b) Single droplet drying of dairy-based systems at spray drying like temperature–time trajectories. *International Journal of Dairy Technology* **77** 1003–1016.

Esmonde-White K, Lewis M, Perilli T, Della Vedova T and Lewis I (2022) Raman spectroscopy in analyzing fats and oils in foods. *Spectroscopy* **2** 34–45.

Farahi R H, Lereu A L, Charrier A M, Kalluri U C, Davison B H and Passian A (2020) Nanomechanics and Raman spectroscopy of in situ native carbohydrate storage granules for enhancing starch quality and lignocellulosic biomass production. *ACS Omega* **5** 2594–2602.

Fitzpatrick J J, Iqbal T, Delaney C, Twomey T and Keogh M K (2004) Effect of powder properties and storage conditions on the flowability of milk powders with different fat contents. *Journal of Food Engineering* **64** 435–444.

Frascareli E C, Silva V M, Tonon R V and Hubinger M D (2012) Effect of process conditions on the microencapsulation of coffee oil by spray drying. *Food and Bioproducts Processing* **90** 413–424.

Fu N, Woo M W and Chen X D (2012) Single droplet drying technique to study drying kinetics measurement and particle functionality: A review. *Drying Technology* **30** 1771–1785.

Gharsallaoui A, Roudaut G, Chambin O, Voilley A and Saurel R (2007) Applications of spray-drying in microencapsulation of food ingredients: An overview. *Food Research International* **40** 1107–1121.

Haas K, Obernberger J, Zehetner E, Kiesslich A, Volkert M and Jaeger H (2019) Impact of powder particle structure on the oxidation stability and color of encapsulated crystalline and emulsified carotenoids in carrot concentrate powders. *Journal of Food Engineering* **263** 398–408.

Höhne S and Gaukel V (2024) Impact of the drying rate on product properties of spray dried emulsions to enable a targeted product design. *Drying Technology* **42** 1–7.

Kim E H-J, Chen X D and Pearce D (2005) Effect of surface composition on the flowability of industrial spray-dried dairy powders. *Colloids and Surfaces B: Biointerfaces* **46** 182–187.

Kurtz T, Haas K, Busom Descarrega J, Meunier V, Schafer O and Heinrich S (2025) The role of pea protein content and carbohydrate molecular weight in the structure and stability of spray-dried emulsions. *Food Hydrocolloids* **166** 111320.

Kwofie F, Lavine B K, Ottaway J and Booksh K (2020) Differentiation of edible oils by type using Raman spectroscopy and pattern recognition methods. *Applied Spectroscopy* **74** 645–654.

Linke A, Hinrichs J and Kohlus R (2020) Impact of the oil droplet size on the oxidative stability of microencapsulated oil. *Journal of Microencapsulation* **37** 170–181.

Malafronte L, Ahrné L, Schuster E, Innings F and Rasmuson A (2015) Exploring drying kinetics and morphology of commercial dairy powders. *Journal of Food Engineering* **158** 58–65.

Masters K (2002) *Spray Drying in Practice*, Charlottenlund: SprayDry-Consult International ApS.

Mujumdar A S (2015) *Handbook of Industrial Drying*, 4th edn Boca Raton, FL: CRC Press.

Nešić S and Vodnik J (1991) Kinetics of droplet evaporation. *Chemical Engineering Science* **46** 527–537.

Nuzzo M, Millqvist-Fureby A, Sloth J and Bergenstahl B (2015a) Surface composition and morphology of particles dried individually and by spray drying. *Drying Technology* **33** 757–767.

Nuzzo M, Sloth J, Brandner B, Bergenstahl B and Millqvist-Fureby A (2015b) Confocal Raman microscopy for mapping phase segregation in individually dried particles composed of lactose and macromolecules. *Colloids and Surfaces A: Physicochemical and Engineering Aspects* **481** 229–236.

Rodrigues Júnior P H, de Sá Oliveira K, Almeida C E R, de Oliveira L F C, Stephani R, Pinto M S, Carvalho A F and Perrone Í T (2016) FT-Raman and chemometric tools for rapid determination of quality parameters in milk powder: Classification of samples for the presence of lactose and fraud detection by addition of maltodextrin. *Food Chemistry* **196** 584–588.

Routh A F and Zimmerman W B (2004) Distribution of particles during solvent evaporation from films. *Chemical Engineering Science* **59** 2961–2968.

Schutyser M A I, Both E M, Siemons I, Vaessen E M J and Zhang L (2019) Gaining insight on spray drying behavior of foods via single droplet drying analyses. *Drying Technology* **37** 525–534.

Shamaei S, Kharaghani A, Seiiedlou S S, Aghbashlo M, Sondej F and Tsotsas E (2016) Drying behavior and locking point of single droplets containing functional oil. *Advanced Powder Technology* **27** 1750–1760.

Taboada M L, Schäfer A, Karbstein H P and Gaukel V (2021) Oil droplet breakup during pressure swirl atomization of food emulsions: Influence of atomization pressure and initial oil droplet size. *Journal of Food Process Engineering* **44** e13598.

Tan L H, Chan L W and Heng P W S (2005) Effect of oil loading on microspheres produced by spray drying. *Journal of Microencapsulation* **22** 253–259.

Vega C and Roos Y H (2006) Invited review: Spray-dried dairy and dairy-like emulsions—Compositional considerations. *Journal of Dairy Science* **89** 383–401.

Walton D E and Mumford C J (1999) Spray dried products—Characterization of particle morphology. *Chemical Engineering Research and Design* **77** 21–38.

Wang Y, Che L, Selomulya C and Chen X D (2014) Droplet drying behaviour of docosahexaenoic acid (DHA)-containing emulsion. *Chemical Engineering Science* **106** 181–189.

Werner S R L, Jones J R and Paterson A H J (2007) Stickiness of maltodextrins using probe tack test during in-situ drying. *Journal of Food Engineering* **80** 859–868.

Zhang S, Zhang Z, Lin M and Vardhanabhuti B (2012) Raman spectroscopic characterization of structural changes in heated whey protein isolate upon soluble complex formation with pectin at near neutral pH. *Journal of Agricultural and Food Chemistry* **60** 12029–12035.

APPENDIX A

Overview of the Sauter mean diameter and $x_{10,3}$ values of the particle size distributions of all spray-dried powders..

	Maltodextrin				Mod. Starch			
	$\bar{x}_{1,2}$		$x_{10,3}$		$\bar{x}_{1,2}$		$x_{10,3}$	
	180°C	220°C	180°C	220°C	180°C	220°C	180°C	220°C
20 wt%	77.98	67.87	30.66	27.00	40.68	38.03	22.86	20.91
40 wt%	69.82	80.64	23.39	35.67	43.39	35.67	25.83	26.71
60 wt%	70.13	88.43	30.79	36.26	42.22	41.73	25.08	24.82

APPENDIX B

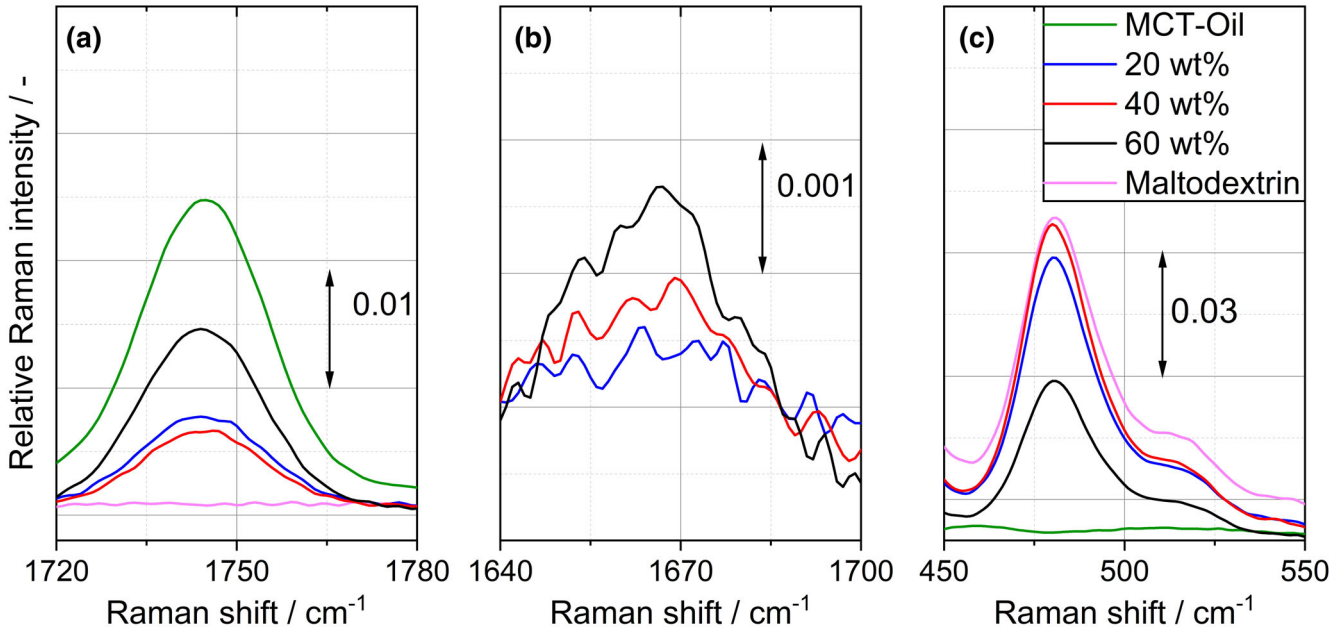

Characteristic bands of the Raman spectra for MCT-oil (a), WPI (b), and Maltodextrin (c) for particles dried with different oil concentrations. Particles were dried at $T_{start} = 120°C$ and $T_{end} = 65°C$.

APPENDIX C

Equation for the calculation of the distance of a measured Raman intensity from a homogeneous distribution.

For the calculation of the distance of the measured Raman intensity from the Raman intensity of a homogeneous distribution, the following equation is used:

$$\text{Distance} = 1 - \frac{I_S - I_{MD}}{I_{HD} - I_{MD}}$$

with I_S being the Raman intensity of the sample at 1744 cm^{-1}, I_{MD} being the Raman intensity of maltodextrin at 1744 cm^{-1}, and I_{HD} being the theoretical Raman intensity of a homogeneous distribution at 1744 cm^{-1}.

APPENDIX D

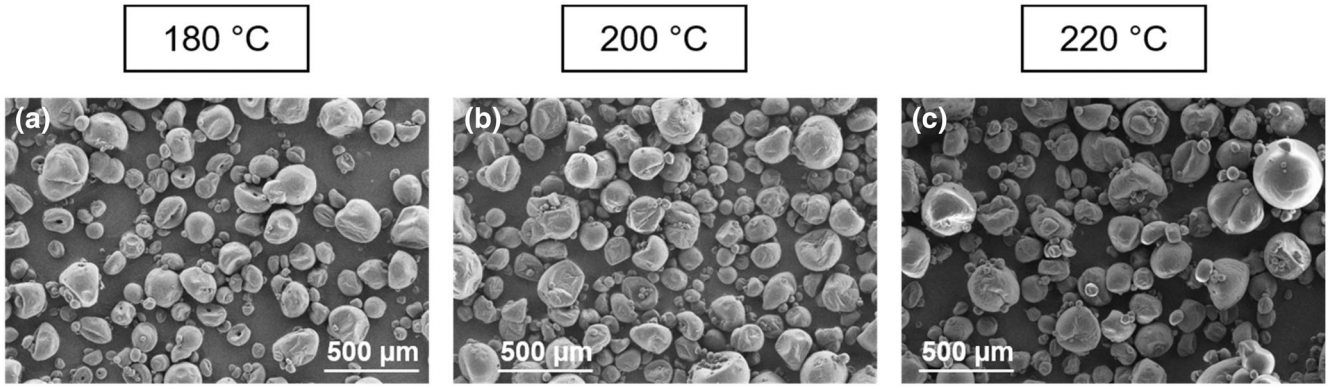

SEM micrographs of spray dried powders containing maltodextrin, WPI and 40 wt% MCT-oil for inlet air temperatures of 180°C (a), 200°C (b), 220°C (c). Outlet air temperature was kept constant at $T_{out} = 85°C$ (SEM images acquired by the Electron Microscopy Laboratory at the Karlsruhe Institute of Technology).

APPENDIX E

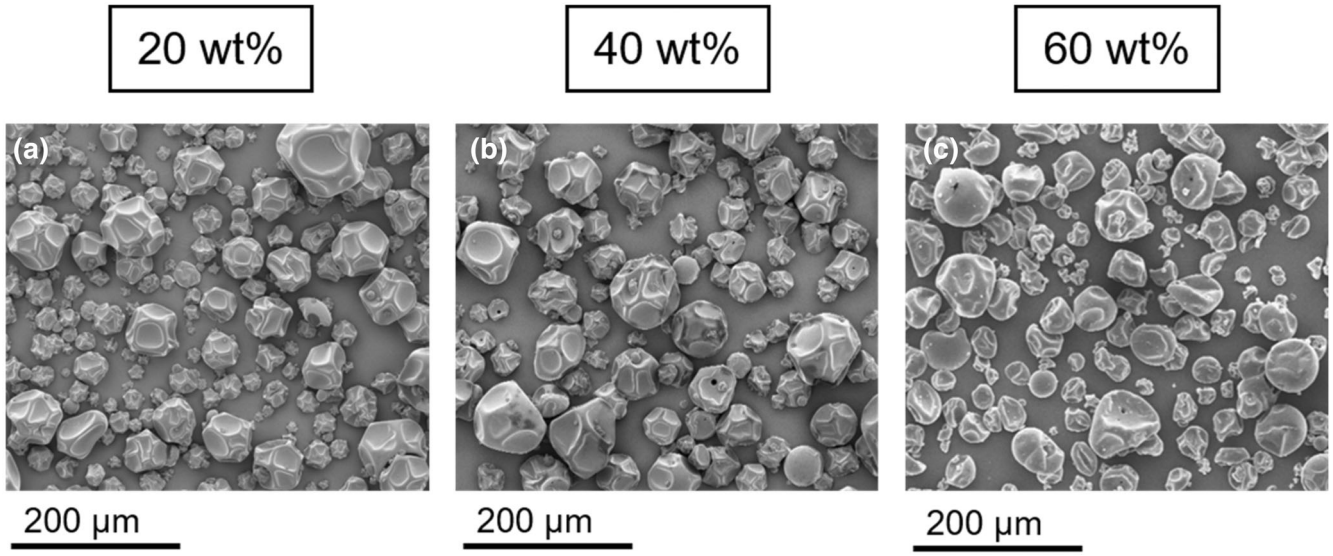

SEM micrographs of spray dried powders containing modified starch and 20 wt% (a), 40 wt% (b) and 60 wt% (c) MCT-oil. Drying temperatures were kept constant at $T_{in} = 180°C$ and $T_{out} = 85°C$ (SEM images acquired by the Electron Microscopy Laboratory at the Karlsruhe Institute of Technology).

APPENDIX F

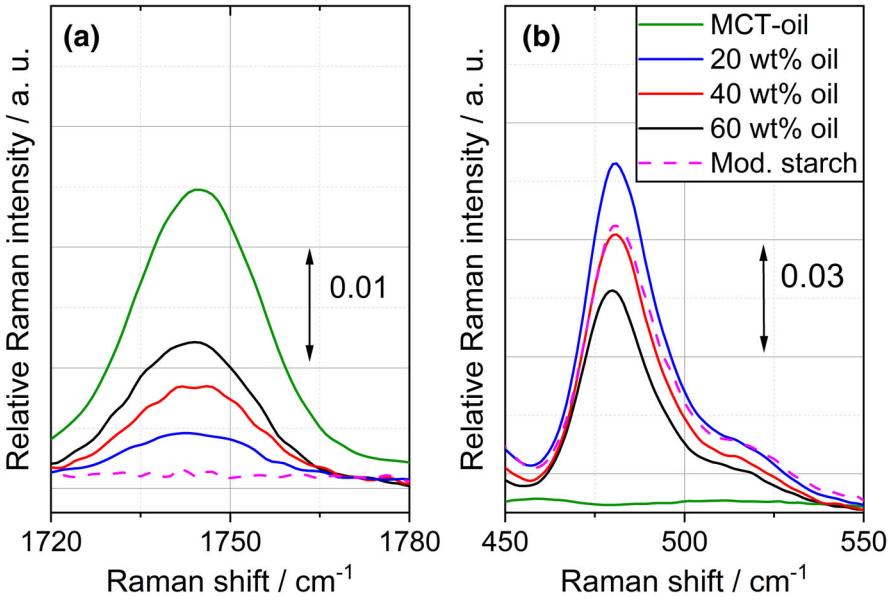

Characteristic bands of the Raman spectra for MCT-oil (a) and modified starch (b) for particles dried with different oil concentrations. Particles were dried at $T_{start} = 100°C$ and $T_{end} = 65°C$.